11

Full Scale Pedestrian Impact Testing with PMHS: *A Pilot Study*

J. R. Kerrigan,
C.Y. Kam, D.C. Drinkwater, D.B. Murphy, C. Arregui,
S. Millington, G. Teresinski, J.R. Bolton, J.R. Crandall
B. Deng, J.T. Wang, C. Kerkeling, and W. Hahn

ABSTRACT

The complexity of vehicle-pedestrian collisions necessitates extensive validation of pedestrian computational models. While body components can be individually simulated, overall validation of human pedestrian models requires full-scale testing with post mortem human surrogates (PMHS). This paper presents the development of a full-scale pedestrian impact test plan and experimental design, and some results from a pilot experiment. The test plan and experimental design are developed based on the analysis of a combination of literature review, multi-body modeling, and epidemiologic studies. The proposed system has proven effective in testing an anthropometrically correct rescue dummy in multiple instances, and in one test with a PMHS.

INTRODUCTION

Pedestrian injury is a real public health problem. Sixty-five percent of the 1.17 million people that die in road traffic accidents worldwide each year are pedestrians (World Bank, 2002). While the percentage of pedestrian fatalities is much higher in developing nations than in industrialized nations, pedestrians still make up 11%-30% of road traffic fatalities in the US, the European Union, and Japan (NHTSA, 2003; CARE, 2002; NPA, 2003).

Although pedestrians are frequently killed as a result of a vehicle collision, the number of pedestrians injured actually outweighs the number of fatalities by 15 to 1 in the United States (NHTSA, 2003). Due to the severity of even low speed collisions, pedestrian injuries are often life-threatening and debilitating. According to the Pedestrian Crash Data Study (PCDS) data, 35% of AIS 3-6 injuries occur in pedestrian collisions at speeds below 30 km/h (19 mi/h) (Chidester and Isenburg, 2001). Given the complexity and severity of these injuries, medical and traffic safety professionals are faced with the

challenge of finding ways to mitigate their degree and frequency, and ultimately to increase pedestrian survival rates.

In line with this goal, researchers are currently working to develop both computational models and improved dummies with the goals of (1) quantifying pedestrian kinematics and kinetics to further understand pedestrian injury mechanisms, and (2) developing and testing vehicle countermeasures in component-level and full-scale impact situations. The success of these pedestrian surrogate models as tools for countermeasure development is predicated on the biofidelity of the model.

Pedestrian surrogate models need to be validated for biofidelity against PMHS test data in both component-level and full-scale impact tests. Although the numerous full-scale pedestrian impact experiments that have been performed thus far provide a wealth of information regarding design and methodology, most of these studies have been performed using older vehicles having front end geometries not representative of the current vehicle fleet. Differences in front-end vehicle geometry have been shown to influence pedestrian kinematics and injury measures (Meissner et al., 2004). Computational model validation from previous full-scale test studies is further restricted because most studies are limited in the level of detail provided in the data presented.

Detailed kinematic and kinetic data for pedestrian PMHS tested in full-scale impact experiments using late model vehicles will provide the necessary basis for biofidelic validation of pedestrian surrogate models. The complexity of vehicle-pedestrian collisions and the level of detail required in test data necessitate full-scale impact experiments that are both intricate and complex. The purpose of this study is to develop a full-scale pedestrian impact test plan for dummies and PMHS. These tests are designed to accurately reproduce the kinematics and injuries experienced by pedestrians as the result of collisions with vehicles.

This study highlights previous research, epidemiologic data, and multi-body computational simulations in the development of a test system and experimental plan for full scale pedestrian impact testing.

METHODS (TEST PLAN AND SYSTEM DESIGN)

Since the goal of this study is the development of a test plan and experimental design that would allow for full scale pedestrian impact experiments with both dummy and PMHS pedestrian surrogates, the first thing that was considered was the positioning of the subject prior to the vehicle impact.

Pedestrian Stance and Positioning

Three aspects of pre-crash stance were considered for this study: body orientation, leg orientation, and arm orientation.

Body Orientation. The first of these aspects to be considered was which overall body orientation relative to the vehicle (anterior, posterior, or lateral) might be considered most representative of pedestrians in real world collisions. With this goal in mind, epidemiologic data was gathered from the PCDS to further investigate pedestrian stance and position at impact.

The PCDS database was created as a result of the need for reliable data to establish injury criteria for pedestrians and to improve understanding of real world pedestrian crashes (Henary, 2003). The database consists of detailed information on 552 crashes involving pedestrians in six major cities in the United States from 1994-1998. PCDS data provide detailed information regarding the pre-crash and at-crash circumstances of the pedestrian and the vehicle, environmental and scene data, as well as injuries endured by the pedestrians involved. While the PCDS was intended to be a clinical study and was never designed to represent a national sample of US pedestrian crashes, a report summarizing some of the data in the database was presented by Chidester and Isenburg (2001). An additional analysis of the PCDS database was performed for this study by the University of Virginia to better understand pedestrian-vehicle collisions.

PCDS data shows that 75 (14%) pedestrians are impacted on their anterior face, 42 (8%) on their posterior face, 228 (41.3%) on their left side, 178 (32%) on their right side, and 29 (5%) were unknown. When anterior and posterior impacts are grouped together, and left and right side impacts are grouped with lateral impacts (Figure 1), it can be seen that the latter make up for almost 74% of pedestrian collisions.

Chidester and Isenburg (2001) report that 356 (68%) of the struck pedestrians were oriented with their side to the striking vehicle, with 89 (17%) facing the vehicle and 53 (10%) facing away.
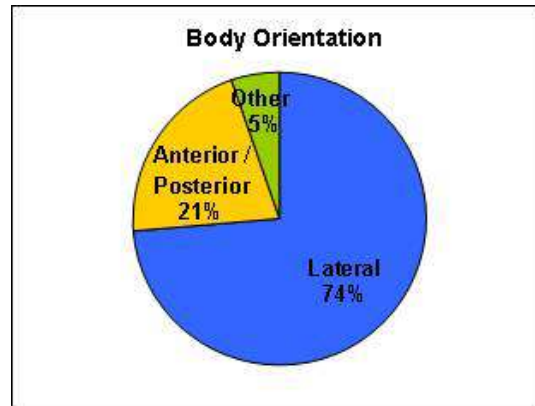

Figure 1: PCDS data showing body orientation at impact.

Also, with respect to the pedestrian's motion prior to any avoidance actions, 453 (87%) of the pedestrians were attempting to cross the roadway (Chidester and Isenburg, 2001). Based on this data, lateral impacts were chosen for this study because it was felt that this orientation was representative of real world accidents as a majority of pedestrians are struck laterally by a vehicle as they are crossing the street.

Leg Positioning. Along with the body orientation, it was necessary to specify a leg orientation (stance) representative of pedestrians in a pre-crash orientation. The PCDS data shows that 31 (6%) of the pedestrians impacted are standing with legs together, 27 (5%) are impacted with legs apart laterally, 362 (65%) were found to be in a gait stance at the time of collision, and 132 (24%) were in some other unknown stance (Figure 2).

Chidester and Isenburg (2001) found that prior to crash, the physical motions of 289 (55%) pedestrians were reported as walking and that 376 (72%) of the pedestrians had one limb forward and apart from the other limb at the time of impact.

Since a majority of pedestrians were found to be walking prior to vehicle collision, the phases that are involved in human gait were examined next. For a given gait cycle, there are two main phases that can be used to describe the entire cycle; a stance phase and a swing phase. The stance phase includes any portion of the cycle in which both limbs are in contact with the ground and can be broken down into three minor stances of its own: a loading stance, a mid-stance, and an unloading (or terminal) stance. At full stride, the start of a human gait cycle may be defined as the point at which the left foot is forward and both feet are supporting the body's weight equally. This is known as mid-stance (Figure 3). As the person continues to move forward, a terminal stance is arrived when the right heel rises up leaving the forefoot in contact with the floor (see "Unload" in Figure 3). Further progress forward is achieved by the toes of the right foot pushing off and finally leaving the ground, initiating the swing phase, in which the right leg swings forward past the left leg until it is about one step length in front. Loading stance is initiated at the point at which the right heel begins to contact the floor, followed by contact of the right forefoot, and finally the right toes. At this point, the pedestrian is once again in mid-stance and has completed one-half of a gait cycle (Figure 3).
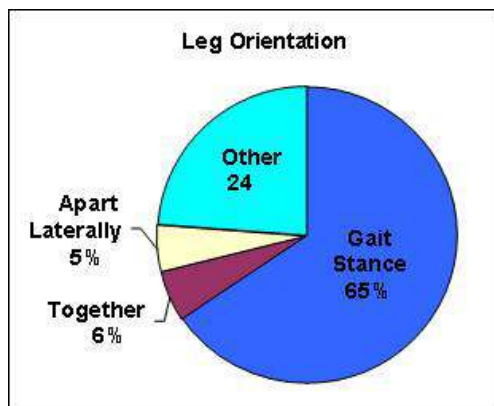
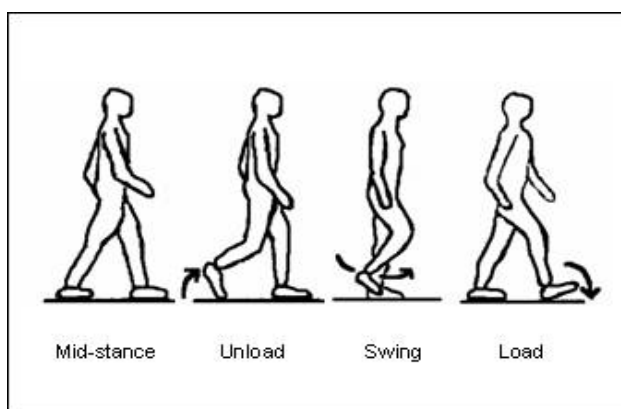Figure 2: PCDS data showing leg orientation at impact.

Figure 3: Phases of gait cycle (half cycle shown).

Preliminary attempts to recreate specific gait stances with PMHS suggested that only two stances could be easily and repeatably obtained: a standing orientation (legs together), and a mid-gait stance with both feet in contact with the floor.

Based on gait analysis alone, the situation where both feet or legs are together occurs only for an instance when one limb swings past the other limb, and at this moment, only one limb is in fact in contact with the ground. On the other hand, total double limb support (both limbs in contact with the ground) is calculated to vary from 16-22% of a full gait cycle (Winter, 1990; Perry, 1992; Allard, 1997). This, however, does not necessarily imply that both limbs are supporting equal amounts of weight.

In previous full-scale pedestrian tests, the majority of the pedestrian subjects were positioned in a way that resembled a walking stance with the struck limb to the rear (Brun-Cassan et al., 1984; Kelleher et al., 1986; Ishikawa et al., 1993; Schroeder et al., 2000). In a few studies such as Farisse et al. (1981) and Billault et al. (1980), the subjects were oriented in a standing position with both limbs close together. However, this stance does not appear to be very common (only 6%) in real pedestrian impacts as seen in the PCDS data.

For several reasons it was decided to position the lower extremities in a mid-stance gait orientation for the current study. Not only is a gait stance the most representative of actual pedestrian collisions, but it also represents a significant proportion of the normal gait cycle (16-22%), and was additionally found to be easily and repeatably achieved with PMHS. With this in mind, the next consideration was whether the struck-side limb should be oriented forward or back. Although a majority of the previous full-scale studies implemented a struck-side limb back orientation, PCDS data suggested no significant difference in occurrence between the two orientations: 127 (23%) pedestrians were struck laterally with struck-side limb back and 143 (26%) pedestrians were struck laterally with struck-side limb forward.

To further investigate the orientation of the struck limb, a multi-body computational study done by Meissner et al. (2004) was reviewed. This study, in which a simulated pedestrian was struck laterally on the left side, not only showed that pedestrian lower limb orientation at impact played a dominant role in the subsequent kinematics of the upper body, but also that orienting the struck-side limb to the rear provided for a counter-clockwise rotation of the pedestrian. This, in turn, resulted in a vehicle loading scenario that was (with regard to the pedestrian) more laterally and anteriorly in aspect, as opposed to lateral and posterior in the case of struck limb forward. Figure 4 shows a sequence of motion for the two cases of struck-side limb forward and struck-side limb back. Differences in upper body rotation can be clearly seen as an effect of initial limb orientation.

Since a primary design objective of the current study was to facilitate the testing of PMHS, an important consideration was the ability to mount instrumentation along on the posterior spine to measure pedestrian kinematics. Since there seemed to be little difference in the orientation of the stuck-side limb from the PCDS data (whether behind or in front of the pedestrian's center of gravity), and the struck limb to the rear orientation provided for the scenario that would potentially cause the least damage to the instrumentation, i.e. counter-clockwise rotation resulting in the anterior aspect of the pedestrian contacting the vehicle, it seemed advisable to adopt this initial orientation for this study.
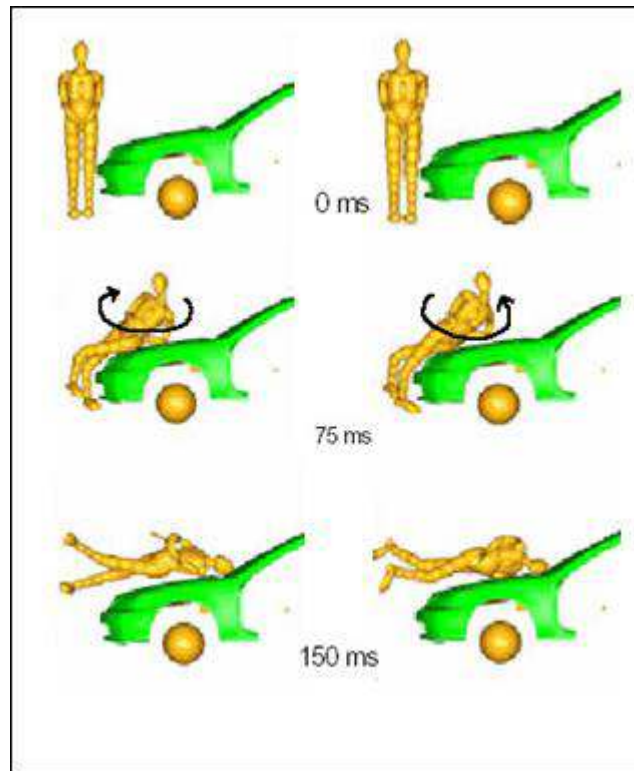

Figure 4: Upper body rotations due to initial leg positioning (Meissner et al., 2004).

In terms of the more detailed criteria for the positioning of the feet, placing them at shoulder width apart laterally (as in normal gait) seemed like a self-evident choice. Specifying the anterior-posterior distance between the feet, however, proved somewhat more problematic due to the variability of stride length depending on the person's height, age, gender, and possibly weight (Winter, 1990). For that reason, experiments with the positioning of PMHS were undertaken to see what step lengths were appropriate for a stable stance. It was subsequently determined that a mid-gait stance with an A-P foot distance of 35 cm to 60 cm (measured toe-to-toe) was suitable. However, the effect of step length on upper body kinematics was unknown, making further analysis necessary.

Multi-body dynamic simulations were performed using MADYMO (Mathematical Dynamical Modeling) Version 6.2 to analyze the difference between long and short step lengths. The 50th percentile

male was used to model the pedestrian in the two mid-gait stances (60 cm and 35 cm steps, with the hands bound in front). The pedestrian, positioned in a lateral facing orientation with its right side toward the vehicle and right leg back, was struck at 40 km/h along the vehicle's centerline. The vehicle used in the simulations was modeled using the geometry of the same experimental mid-sized sedan that was intended to be used in the actual tests. No braking or vehicle pitching was simulated. (The rationale for choosing these conditions will be discussed in subsequent sections.)

The results provided by the simulation are summarized in Figure 5 which shows time history plots of the pelvis rotation (Cardan angle) of the pedestrian for the two step lengths simulated. It can bee seen that pelvis rotations for the two different cases prove quite similar from the time of initial contact with the vehicle bumper to the time of head impact at approximately 125 ms. From 125 ms to approximately 300 ms, slight variations ($\leq 5°$) in pelvis rotation can be seen. It is not until after 300 ms that the pelvis rotation for the two step lengths starts to deviate substantially. Figure 6 shows the superposition of the two pedestrian models at select times.

The simulations show very similar upper body and pelvic rotation for both step lengths up until approximately 310 ms. However, head impact occurs much earlier than 310 ms (roughly 125 ms). Preliminary MADYMO simulations suggest that the time period between initial bumper contact and the eventual head strike is when the pedestrian is accelerated up to the velocity of the vehicle.

The simulations further suggest that it is during this time period that the highest magnitude forces and accelerations are imparted to the pedestrian. It is assumed that it is also during this period that the pedestrian will sustain the most serious injuries caused by collision with the vehicle (this does not include injuries caused by post-collision impact with the ground). Thus, it was decided that the current study need only concern itself exclusively with the kinematics of the pedestrian up to the point of head strike. Since the simulations show only a negligible difference between pedestrian kinematics in the long and short step length cases up to the time of head strike, it was concluded that, for this study, step length (varied between 35 and 60 cm) should not significantly affect pedestrian kinematics.

Since step length did not appear to affect kinematics and positioning PMHS with a step length between 35 cm and 60 cm was not problematic, the size and position of the pedestrian sled foot load plates were specified such that stances between 35 cm and 60 cm could be easily accommodated. (The pedestrian sled will be discussed in a subsequent section.)

Securing The Arms. Following the determination of body orientation and leg stance it became necessary to finalize the pedestrian positioning parameters by taking the effects of the pedestrian's arm position into consideration. Gait analysis has indicated that the arms typically swing in conjunction with lower limb motion, with each upper extremity moving in phase with the opposite lower extremity (Figure 3). However, during a pedestrian collision, the arms may not necessarily follow the normal gait motions. Chidester and Isenburg (2001) reported that pedestrian upper extremity orientation at impact was almost evenly divided: 152 (29%) pedestrians were holding something in their hands or arms, 153 (29%) were not holding anything, 151 (29%) had their arms extended, and the remaining 66 (13%) had their arms in some other unknown manner.
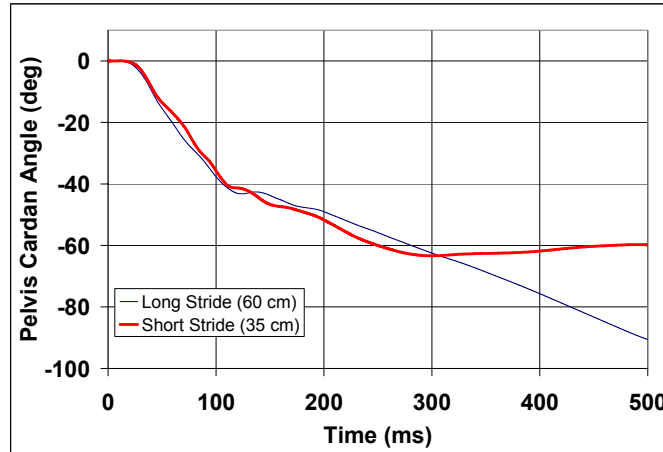
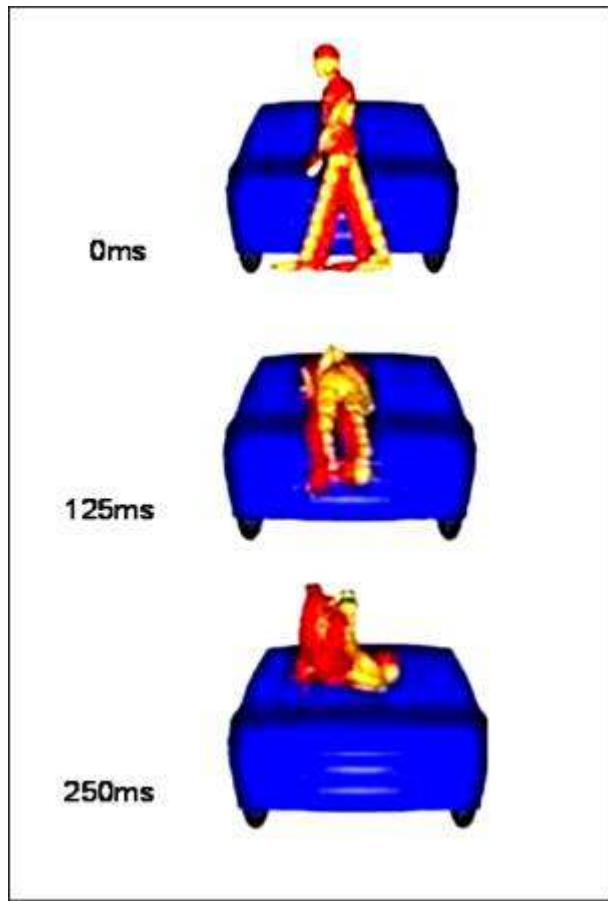Figure 5: Pelvis rotation for long and short steps.

Figure 6: Superposition of subject in long and short step lengths.

Two previous full-scale studies mention accounting for arm position. Kelleher et al. (1986) securely placed the struck arm behind the subjects' back to preclude contact with the hood leading edge. Brun-Cassan et al. (1984) directed the struck arm forward, so as to simulate the normal walking position of a pedestrian and to prevent the upper extremity from getting pinned between the subject's thorax and the vehicle.

The Schroeder et al. (2000) study presents the results and analysis of five full-scale pedestrian impact tests using two different vehicles. Although it is not explicitly stated in the paper, it is obvious from

the drawings depicting the pedestrian kinematics that the arms were positioned at the sides of the subject (not bound) prior to the impact event (Figure 7).
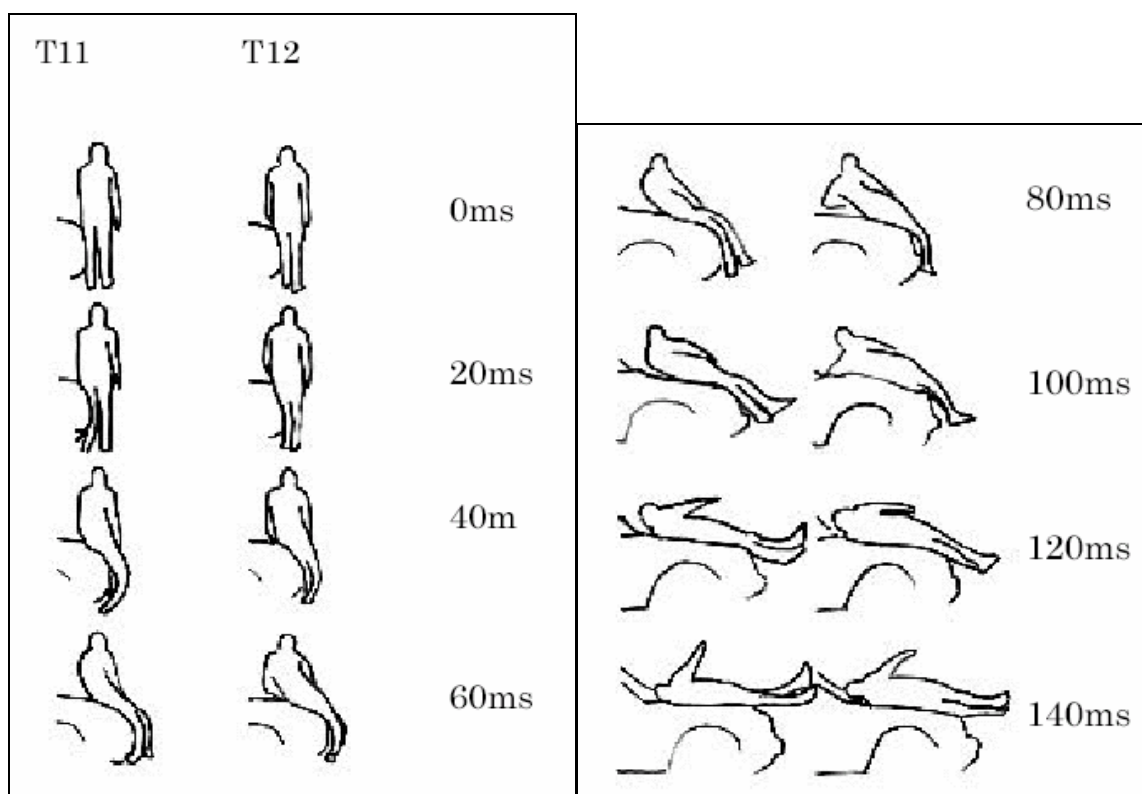

Figure 7: Drawings depicting the kinematic differences between two PMHS tested using the same vehicle from Schroeder et al. (2000).

In two of the tests using the same vehicle (called T11 and T12 in the study), it can be clearly seen that differences in upper-body kinematics occur due to the arm position. In test T11, the left (struck-side) upper extremity does not appear to be pinned between the vehicle and the subject's thorax (Figure 7). However, in test T12, the left elbow clearly makes contact with the vehicle's hood under the pedestrian and this phenomenon alters the subsequent kinematics (Figure 7, test T12, at 80 and 100 ms).

It is hypothesized that if any part of the upper extremity gets pinned between the thorax and the vehicle, there is a potential for a difference in the severity of the head and/or thorax impact. The Schroeder et al. (2000) study shows that if the upper extremities are initially positioned hanging at the sides of the subject, there is only a potential for this "arm pinning" phenomenon, since it occurs in one test but not in the other.

This uncertainty is undesirable in the current study because there is a potential to have completely different upper body kinematics while using the same initial subject position. It seems that the only way to ensure repeatable kinematics of the subjects tested in a full-scale pedestrian impact test is to fix the upper extremities in an orientation that restricts the struck side upper extremity from being pinned between the thorax and the vehicle.

The Brun-Cassan et al. (1984) study makes note of this potential for differing kinematics and gets around it by directing the struck-side forearm forward. Subject positioning in the Brun-Cassan et al. (1984) study is discussed only with respect to the dummy tests. However, PMHS tests are also presented, but there is no discussion of arm position with respect to the PMHS. It is assumed, since the dummy tests are compared to the PMHS tests in the Brun-Cassan et al. (1984) study, that the PMHS were positioned in a similar manner. Although it is likely fairly easy to position the struck side forearm of dummy forward of the torso, it is not clear how to do this with a PMHS.

Thus, for the current study, a plan was devised to try to eliminate the potential for the upper extremity to get pinned between the thorax and the vehicle, i.e. binding the arms of the subject at the wrists anterior to the abdomen. Furthermore, the struck-side wrist will be positioned the farthest from the abdomen and the opposite wrist closest to the abdomen. This serves to position the struck side elbow slightly anterior to the upper-body and could eliminate the potential for the upper extremity to get pinned between the thorax and the vehicle.

Pedestrian Supporting and Release

Once the stance and orientation parameters were established, the next step was to develop a way to hold the subject stationary in the stance and release it just prior to impact from the vehicle.

Reviewing previous full-scale tests, it was discovered that nearly all the subjects tested were suspended by a release mechanism usually attached to the head (Billault et al., 1979; Ashton et al., 1983; Kallieris and Schmidt, 1988; Heger and Appel, 1981), and was typically triggered to release electronically or magnetically prior to impact. The timing of the release was adjusted in order to allow for the subject to be free of the support hardware at the time of impact. This method for suspending and releasing the test subjects seemed ideal because the timing was both accurate and reproducible and the support mechanism minimized any unnecessary mass (ropes, wires, harnesses, etc.).

Based on the success of previous studies, a solenoid release mechanism (Robert A. Denton Inc., Model 5675, Rochester Hills, MI) was chosen for use in this study. Testing of the release mechanism proved that regardless of the amount of weight supported, the release mechanism had a reliably consistent and low response time (between trigger and full release). The release mechanism was mounted just below a load cell, which was used to monitor the exact time in which the subject was released.

The release mechanism needed to be triggered reliably so as to minimize variation in the time between release and initial bumper contact with the subject. To achieve this, an inductive pickup was installed on the sled tracks (the UVA sled system is discussed later) to provide a trigger signal when the vehicle was in the exact same position in each test. The signal from the inductive pickup was sent to a specially designed programmable delay circuit allowing the transmission of the trigger signal to the release mechanism to be delayed in 0.1 ms increments. This delay circuit provided the necessary flexibility to produce a specified delay time (between subject release and initial bumper contact) and to run tests at different speeds without changing the location of the inductive pickup. An anthropometrically correct dummy (a rescue dummy) was used in numerous preliminary full-scale tests to refine the delay circuit setting to provide for a repeatable delay time between subject release and bumper contact.

Preliminary experimentation with PMHS positioning and release had suggested that the lack of stiffness in PMHS joints prevented the PMHS from being able to support any of its own weight, even for a few milliseconds. Thus it seemed desirable to minimize the time between subject release and initial bumper contact to prevent motion of the subject (under gravity) prior to the initial bumper contact. However, the delay time also needed to be long enough to allow for the support rope to fully escape the grip of the solenoid release mechanism. Preliminary tests with the dummy suggested that a delay time of approximately 35 ms was appropriate for a vehicle speed of 40 km/h. (Vehicle speed for the current study is discussed later.)

The release mechanism was attached to a wire rope that ran through a winch-pulley system constructed directly above the pre-impact location of the subject. In addition to supporting the test subject, this allowed for the test subject to be raised and lowered as required for the successful performance of the positioning process (Figure 8).
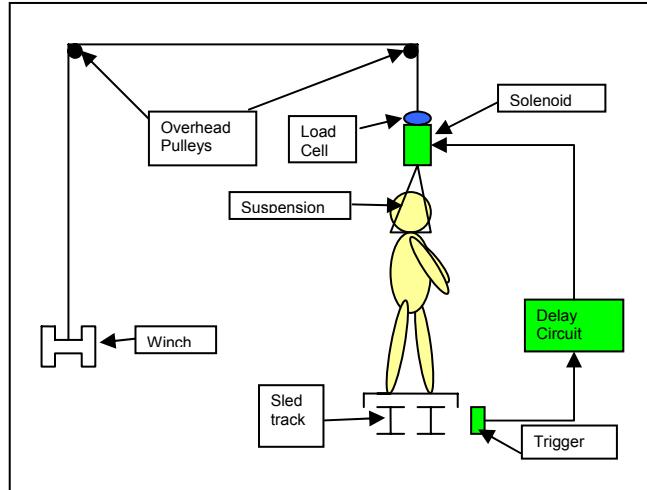
Figure 8: Schematic of test subject being supported and suspended by solenoid dropping mechanism.

In conjunction with the release mechanism itself, a method for suspending the subject from the release mechanism was necessary in order to maintain the desired stance. In the tests performed by Pritz et al. (1975), no electromagnetic release mechanism was used, but rather, the subjects were braced and hung on guy wires. The subjects were supported in a standing position by a brace that consisted of an aluminum rod (3/8" diameter) that ran vertically along the entire length of the body and the impacted limb. As the car impacted the subject, the rod would slip off the guy wires and become free. Although the subject was setup so that it supported nearly all of its body weight on the impacted limb, the subject did not become free from the support structure until after impact from the vehicle. While this support methodology permitted significant load-bearing on the struck-side limb, the external hardware seemed likely to affect both pedestrian kinematics and stiffness. Thus, body braces and other harnesses were avoided. Instead, a simple support system was chosen that consisted of two straps: one that went on the head and one that went around the torso (Figure 9).
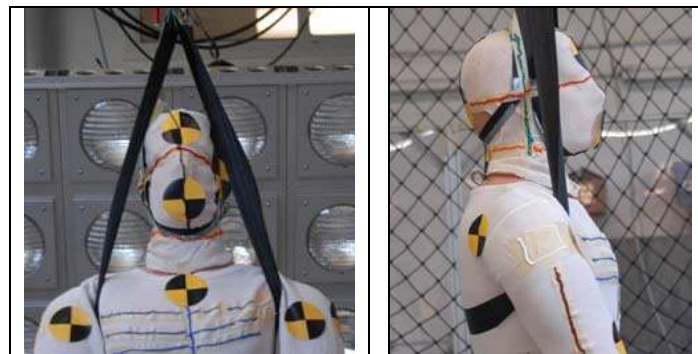

Figure 9: Support system showing anterior and lateral view of seatbelt straps
supporting around the head and torso of dummy subject.

Seatbelt material was chosen for the straps because of its light weight, high strength, and durability. A slit was cut in the head strap and the head was slipped through. One-half of this strap supported the chin while the other half supported the back of the head. The strap for the torso went across the back, under the arms, and up anterior to the shoulders (Figure 9). Going around the back rather than the front helped to keep the body in an erect standing position. Both ends of the straps were outfitted with grommetted holes which allowed them to be tied together with climbing rope. The grommets provided flexibility for different subject sizes as well as the ability to change the portion of the pedestrian's weight supported by each of the two straps (Figure 10). This allowed the torso strap to be adjusted so as not to overload the neck by supporting too much of the subject's mass with the head strap. The other end of the rope was then attached to the solenoid release mechanism.

Figure 10: Seatbelt straps with brass grommets on the ends tied with
climbing rope and attached to solenoid dropping mechanism.

Vehicle Interaction and Braking

With the pedestrian fully supported in the prescribed stance, the subject was ready to be impacted with a vehicle. But before this could happen, the conditions at impact would require prescription, particularly the impact speed and whether or not to include braking effects.

From a review of the study of PCDS data done by Chidester and Isenburg (2001), it was determined that nearly 70% of pedestrian accidents in the United States occur at or below speeds of 30 km/h, with only 20% occurring at speeds of 30 to 45 km/h. However, it was interesting to note that the number of AIS 3-6 injuries rose substantially at impact speeds over 30 km/h. It was shown by Chidester and Isenburg (2001) that the majority of pedestrian injuries from collisions between 16 km/h and 30 km/h were AIS 1-2 injuries whereas the majority of injuries from collisions between 31 km/h and 45 km/h were AIS 3-6. Since life-threatening injuries appear at a much higher frequency in collisions between 31 km/h and 45 km/h, and since the European Enhanced Vehicle Safety Committee guidelines suggested that testing for the protection afforded to pedestrians by safety measures designed into the fronts of vehicles should be performed at 40 km/h (EEVC, 1998), an impact speed of 40 km/h (25 mi/h) was chosen for this study.

In addition to the vehicle speed, the issue of whether or not braking of the vehicle should occur at impact was debated. Many of the previous full-scale tests used early production vehicles that had the front suspensions clamped or tightened in order to simulate the effects of braking (vehicle pitch) without requiring the actual application of braking action before impact (Pritz et al., 1975; Billault et al., 1980). This was an effective means of simulating vehicle diving pitch without sacrificing the consistency of speed and angle prior to impact.

In one set of tests, Heger and Appel (1981) applied braking prior to impact in order to recreate the downward pitch experienced during hard braking. However, the difficulties associated with maintaining consistency with regards to both vehicle impact velocities and pitch angles would seem to argue against the adoption of this strategy.

A vast majority of the tests that were performed included the application of braking at the time of impact (Bourret et al., 1979; Billault et al., 1980; Ashton et al., 1983; Cavellero et al., 1983; Schroeder et al., 2000). A select few utilized braking at 200-300 milliseconds after the initial impact (Brun-Cassan et al.,

1984; Kallieris and Schmidt, 1988; Pritz et al., 1975), probably to stop the vehicle at the end of the test. In both the previously mentioned MADYMO simulations in which step length was investigated and in our preliminary dummy tests, it was determined that in the case of a typical mid-sized sedan, head strike occurs around 120-130 ms. Since it had already been determined that the current study would concern itself only with pedestrian kinematics occurring up to and including the time of head strike, decelerating the vehicle at a time between 200 ms and 300 ms after initial contact seemed reasonable for establishing the end of the test.

Although most previous studies employed braking in some form or another during the vehicle-pedestrian interaction, the question of whether the current proposed testing should employ braking or brake pitching remained undecided. In an attempt to address this question, and investigation of the variability of braking in real world pedestrian collisions was conducted. PCDS data showed that 298 (54%) cases of pedestrian collisions involved braking of some sort, 207 (37.5%) cases involved no braking, and 47 (8.5%) cases were unknown or involved some other form of avoidance maneuver (Figure 11).
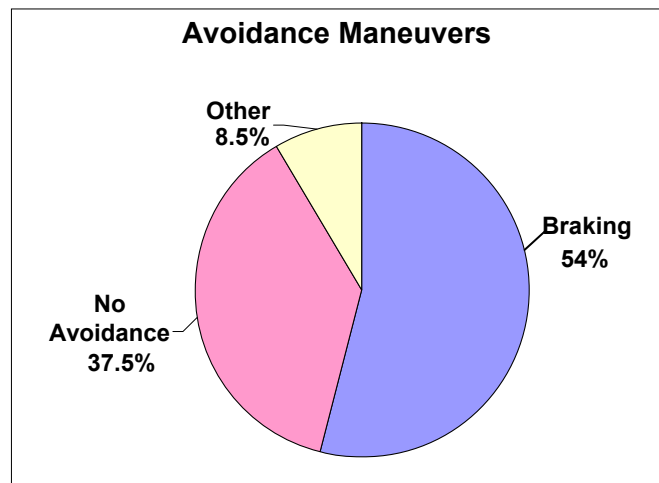

Figure 11: Breakdown of driver maneuvers in pedestrian –vehicle collisions (552 cases).

Even though the cases of braking outnumbered that of no avoidance, the PCDS database further broke the braking category down into the subcategories of braking with and without brake lockup, and a combination of braking and steering to the right or left. Also, the amount of braking applied by the driver can vary along with the braking power of the individual vehicles. With so much variability involved in the braking cases, the identification of a single appropriately representative braking condition was seen to be problematic at best.

Previous studies and PCDS data seem to show a split between cases of braking and no braking and thus the question of whether braking alone had an effect on the kinematics of the pedestrian required further investigation. As a result, MADYMO simulations were performed to model the conditions of braking (0.7 g) at the time of bumper contact and also of no braking. These simulations were set up using the same conditions as those described above for evaluating pedestrian step length, but used only the short step length and the additional condition of the hands bound in front of the body. These simulations did not include the effect of pitching.

The kinematic comparison of the pedestrian with and without braking is shown in Figure 12. The two cases produced very similar results up until head impact, approximately 125 ms after initial contact. Minor differences in body rotation were seen after head impact with the vehicle but were again considered insignificant for the proposed tests.

Since 46% of the PCDS cases did not include braking and because the MADYMO simulations showed only negligible kinematic differences between an impacting vehicle that is braking and one that is not braking, it was decided to perform the tests without braking. An additional implication of this decision was that the need for pitching was eliminated. (Eventual braking of the vehicle is, of course, still necessary at some time after head impact in order to decelerate the vehicle. This will be discussed in greater detail in a later section.)
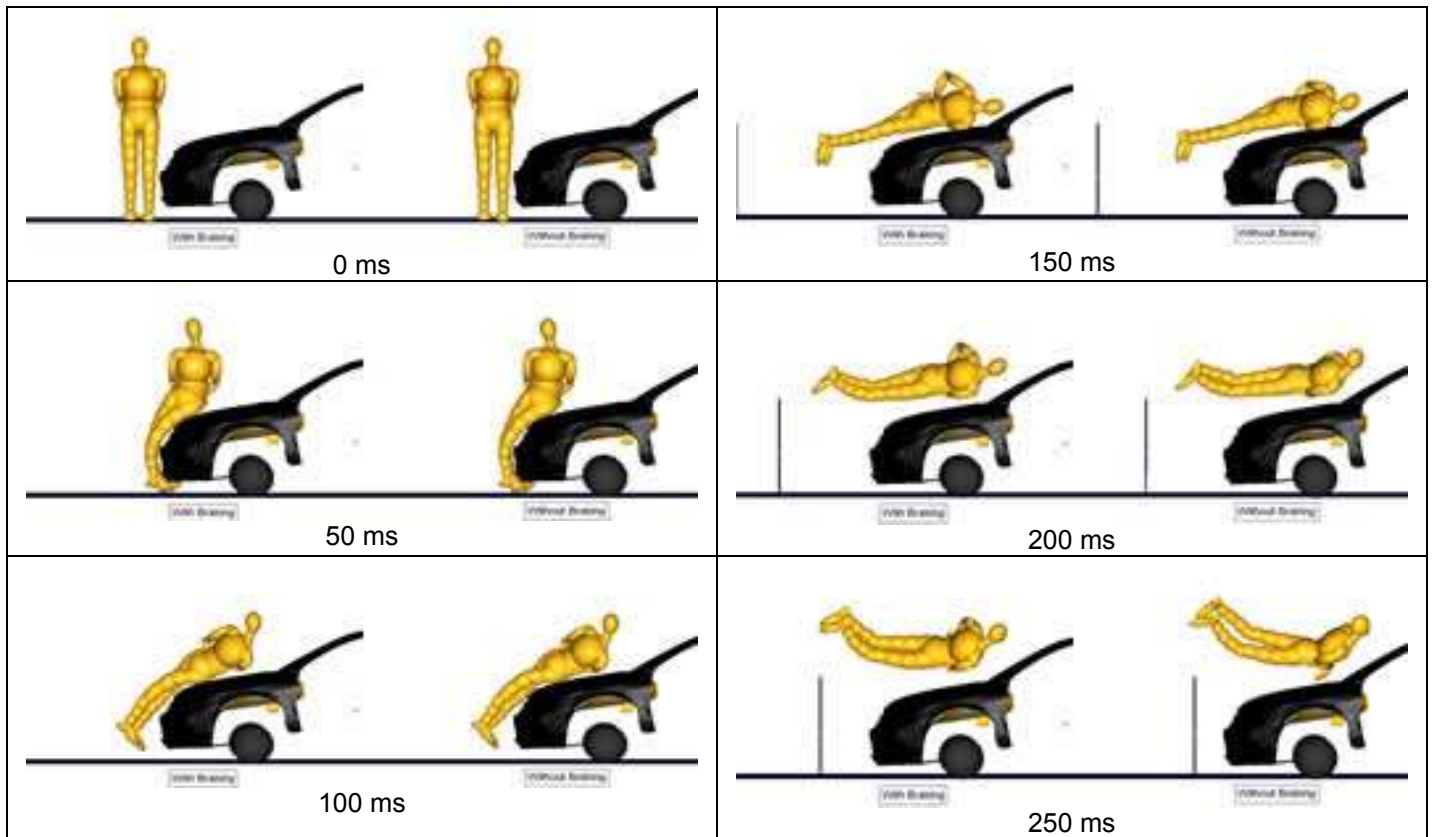
Figure 12: Braking (left) versus no braking (right).

Test Sled and Vehicle Design

Following the specifications of the pedestrian stance and vehicle conditions, it became necessary to integrate the vehicle into the test system. Since the plan was to test an actual vehicle (the mid-sized sedan mentioned above), previous studies were again reviewed to gain insight on how production vehicles were modified for testing.

Several of the previous full-scale tests used production vehicles that were released on an inclined ramp in order to achieve the desired impact speed (Bourret et al., 1979; Cesari et al., 1980; Billault et al., 1980). These vehicles were unmodified except for the brake system, which was rigged so that braking could be applied at some predetermined time and rate. Clamping of the front suspensions was also added in the tests performed by Billault et al. (1980) to produce the pitching effect. This scenario was comparable to real-world collisions in that the vehicle underwent very few modifications prior to the test. However, it also required a sizeable test space to accommodate a ramp large enough to get the vehicles up to the desired speed.

Since the limited amount of space available at the UVA test facility unfortunately rendered the utilization of an acceleration ramp for whole vehicles infeasible, and since a deceleration sled system was already in place at the facility, it seemed obvious to attempt to find a way to perform the tests with the existing system. Since space limitations abrogated the use of whole production vehicles (as were used in most previous studies), but the advantages in real-world fidelity associated with performing the study with an actual vehicle continued to be compelling, it was decided to section the vehicle and mount it on the existing UVA sled system.

Vehicle Buck. For the current study, the front end of an experimental mid-sized sedan was sectioned at the B-pillar leaving only the front half of the vehicle. The wheels were then removed and the suspension was rigidly locked in a neutral position. A rigid base frame was then welded in place under the vehicle to facilitate buck mounting to the test sled. Ballast bars and other weights were added to the vehicle buck until the mass of the vehicle and sled was equal to the curb weight of the vehicle including two passengers (AM50) and a full tank of gasoline.

The vehicle buck was further modified to include two load cells used to facilitate bumper force calculation. The crush boxes or deformable elements on which the bumper beam was mounted were removed. Since these structures were designed to absorb energy (by crushing) during frontal vehicle-to-vehicle collisions, it was assumed that they would act as rigid structures during pedestrian collisions. Thus the structures were cut and modified to hold two uniaxial load cells (Sensotec, Model 41, Columbus, OH) without modifying the original geometry. The vehicle buck and sled were then mounted to the sled tracks of the UVA sled system.

UVA Sled System. The sled system at the University of Virginia is a pneumatically operated deceleration sled with the sled tracks above the floor level of the laboratory. A pneumatic piston is launched which in turn pulls a cable that is attached to a vehicle buck. The vehicle buck is accelerated down the tracks until it reaches the desired impact velocity at which time the impact with the pedestrian occurs. A hydraulic piston is situated at the end of the tracks to decelerate the vehicle to a stop. The internal orifice array of the hydraulic piston was configured to yield a constant deceleration of 6 g over a 4 ft (1.22 m) stroke. A schematic of the sled and general impact system is shown in Figure 13.

In order to determine the initial location of the subject, a decision as to how long to allow the interaction between the subject and the vehicle to occur was required. Some previous studies (Brun-Cassan et al., 1984; Kallieris and Schmidt, 1988; Pritz et al., 1975) terminated the individual tests by braking the vehicle 200-300 ms after bumper contact. Similarly, for the tests described herein, a time of 250 ms after the initial contact was chosen as the test end point. Continuing the test after the predicted head strike (~125 ms) permits validation of the assumption that the highest magnitude loading of the subject will occur between bumper contact and head strike, and also allows for a margin of error in the predicted time of head strike.
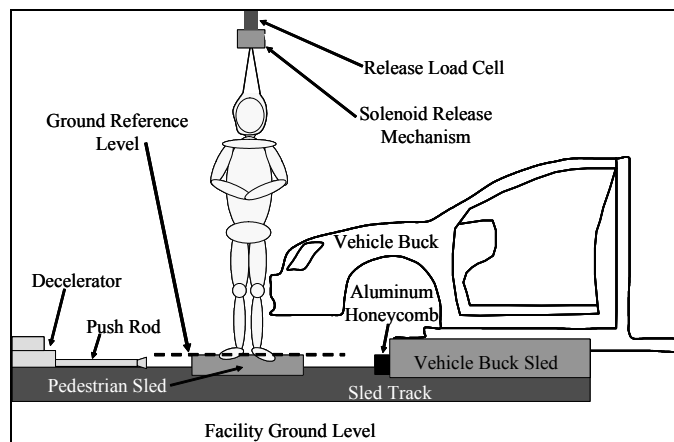

Figure 13: Sled schematic (not drawn to scale).

If the vehicle continued at 11.1 m/s (40 km/h) throughout the entire 250 ms interaction time, the vehicle travel would be approximately 2.8 m (9.1 ft). Thus it was determined that the appropriate position for the subject would be a location on the sled tracks such that the point at which the bumper contacted the subject's lower extremity was 2.8 m from the point where the vehicle contacted the hydraulic decelerator.

Since the vehicle was mounted on sled tracks, the original bumper height from ground reference level (above the top surface of the sled tracks) was no longer valid. Therefore, a method to keep this ground reference level and still allow for the full functionality of the sled system was necessary.

Pedestrian Sled. A pedestrian sled was consequently constructed on the sled tracks to maintain the correct reference bumper height as well as to provide a platform on which the test subject would be positioned. On the top surface of the pedestrian sled, two load cells (Model RL 1260, Rice Lake, WI) were mounted below two square platforms designed to support the subject's feet (Figure 14).

Figure 14: Pedestrian sled platform.

The platform-load cell structures were designed to accommodate stances ranging from the short step length (35 cm) to long step length (60 cm). The load cells monitored the weight distribution of the suspended subject before and after release. Plywood was used as the finishing surface for the square platforms. Simple friction tests showed that the plywood had similar friction coefficients as the asphalt on nearby roads. However, preliminary dummy tests suggest that the surface may not be a factor as the feet are typically lifted completely off the surface soon after bumper contact (Figure 15).
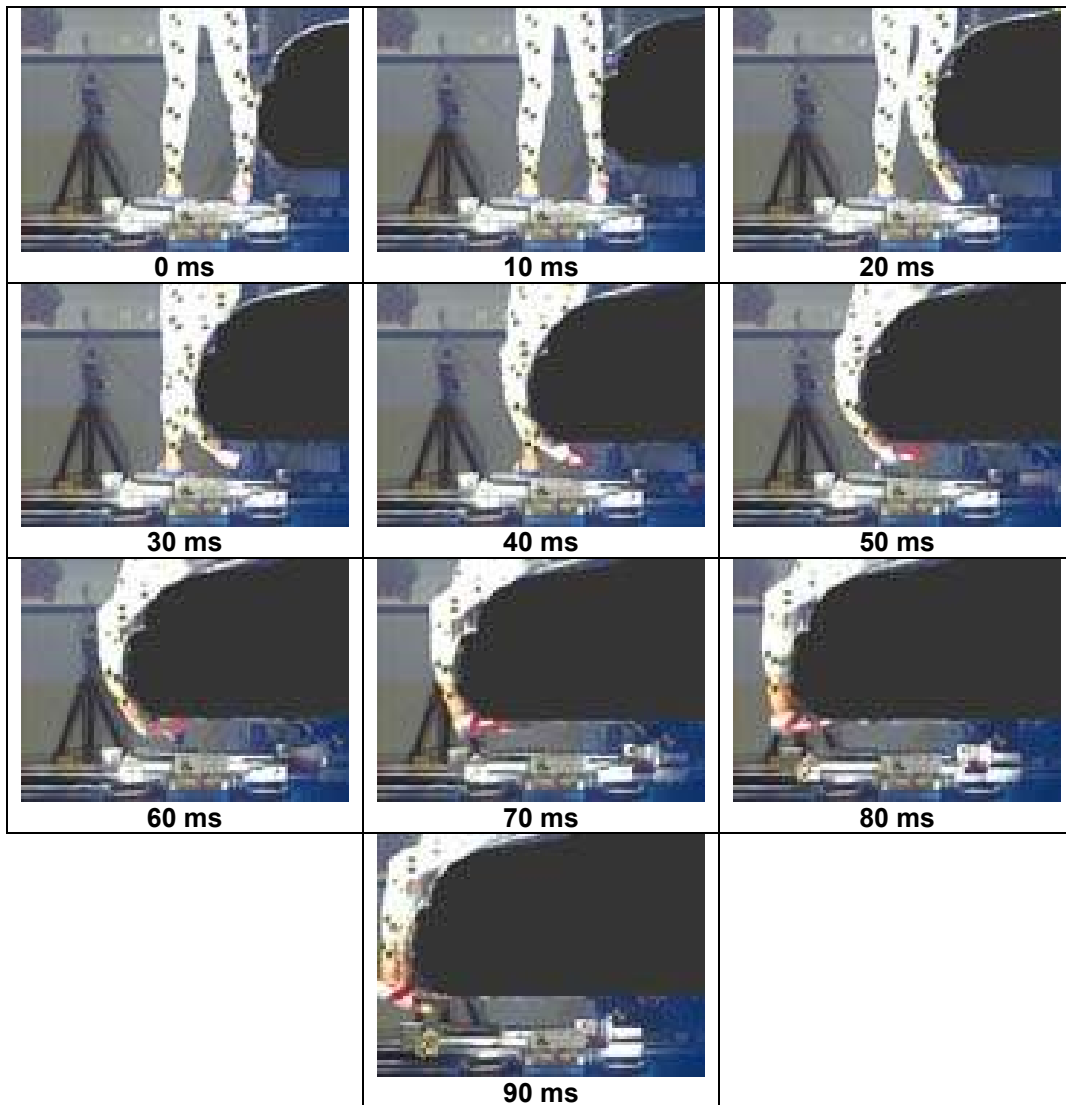
Figure 15: Pedestrian sled interaction at impact during a preliminary full scale test with the rescue dummy.

This can be explained due to the fact that although the pedestrian subject is free at the time of impact, only a small percentage of its weight is supported through the lower extremities. Hence the amount of shear forces due to friction will be substantially lower.

In order for the pedestrian sled to accurately reproduce the characteristics of the road, it has to remain stationary on the track until the feet are no longer in contact with the foot platforms. However, it also has to be able to slide when the vehicle sled contacts it so as not to restrict the vehicle's motion. To achieve this, clamp-style "brakes" were added to the sled track surface just behind the leading sled shoes (Figure 16).
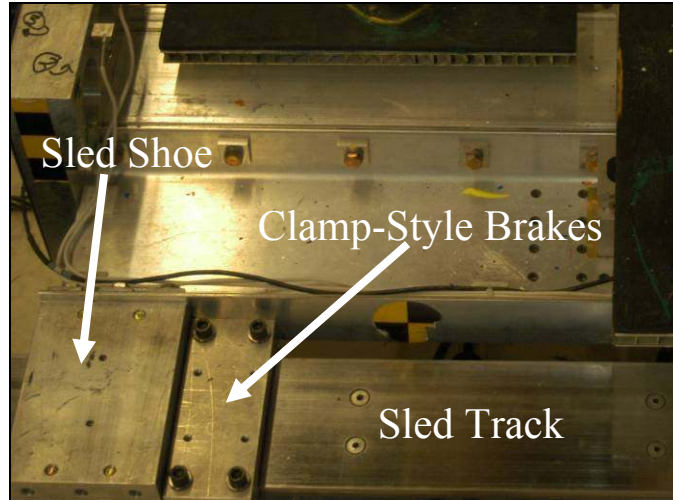
Figure 16: Pedestrian sled with clamp-style brakes.

During a test, the pedestrian sled stays stationary as the test subject is struck. About 45 ms after the initial bumper contact, the subject's feet lose contact with the foot plates. Approximately 15 ms later, the vehicle sled makes contact with the pedestrian sled. At the interface between the vehicle sled and the pedestrian sled, aluminum honeycomb was mounted on the vehicle sled side to provide energy absorption to attenuate the initial acceleration of the pedestrian sled. The honeycomb crushes while the pedestrian sled is accelerated from about 60 ms to about 90 ms after the initial contact (Figure 15). The honeycomb becomes fully crushed at about 90 ms and the pedestrian sled and vehicle sled become coupled and travel together.

The length of the pedestrian sled was designed to match the overhang distance of the front bumper of the buck to the front of the vehicle sled. Thus, once the pedestrian sled and the vehicle sled are coupled, the decelerator interface on the pedestrian sled will be directly below the bumper's leading edge. The distance between the point where the bumper first contacts the subject's lower extremity and the tip of the decelerator push rod could then be specified as the 2.8 m distance mentioned in the previous section.

After the vehicle-pedestrian interaction, the pedestrian sled and vehicle sled, now coupled together, begin the deceleration phase. This begins when the decelerator interface on the pedestrian sled contacts the tip of the decelerator push rod. The vehicle and pedestrian sleds decelerate at about 6 g while the subject, still moving at approximately 11.1 m/s, is lofted off of the front of the vehicle. A subject catching mechanism needed to be implemented to prevent further injury to the subject upon release from the vehicle.

Catching Mechanism

In some previous studies, not much care was given to the prevention of further injuries to the pedestrian subject as a result of contact with the ground. In many of these cases, the subject was fully thrown from the vehicle after braking was initiated and was allowed to hit the ground (Bourret et al., 1979; Billault et al., 1980; Ashton et al., 1983; Cavallero et al., 1983; Brun-Cassan et al., 1984). The reasoning behind this may be to simulate real world collisions where pedestrians are struck by vehicles and then thrown to the ground. PCDS data imply that 31.9% of pedestrian injuries are from secondary road impacts. However, as mentioned earlier, for the first series of tests that will use the current experimental design, the only concern is with pedestrian interaction with the colliding vehicle (up to the time of head strike) and not with any secondary impacts the pedestrian may have with the ground. Thus a full-thrown test scenario is not ideal.

Previous tests have been performed where the secondary impact with the ground was eliminated using padded areas and padded netting to catch the subjects as they were thrown from the vehicle (Pritz et al., 1975; Kallieris and Schmidt, 1988; Schroeder et al., 2000). These padded "catchers" greatly reduced injuries not associated with the initial impact while still allowing the entire pedestrian-vehicle interaction to take place.

For these tests, it was essential to prevent the subject from contacting the ground after initial impact in order to limit the injuries produced to those associated with the primary impact alone and also to prevent

any damage to instrumentation. It was therefore realized that a catching system would be required to allow the subject to gradually come to rest after being thrown off of the vehicle. MADYMO simulations created for the no braking scenario (described in the Vehicle Interaction and Braking section) were used as a basis to help determine the design of the catching mechanism. Of primary interest was the angle at which the pedestrian subject would be projected from the vehicle at the end of the deceleration phase (Figure 17).

The catching mechanism was designed with this angle in mind so that the best distribution of energy absorption could be attained. It was deemed desirable that the subject enter the catching mechanism as soon as the vehicle was completely stopped in order to decrease the unpredictability of the kinematics. Because the pedestrian sled was designed to fit under the overhang of the buck, the catching mechanism was built on top of the decelerator so that the front bumper of the vehicle would be flush with the catcher platform at the end of the deceleration phase.
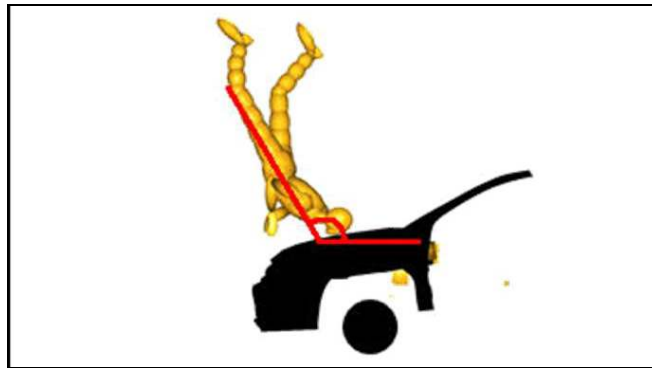

Figure 17: MADYMO simulation showing angle of subject at end of deceleration (120˚ @ 500ms).

In order to accomplish this, a 12 ft x 13 ft (3.66 m x 3.96 m) steel frame was mounted on a steel base frame 3 ft (~1 m) above the sled track. The base frame was covered with plywood to create a platform. The angle of the steel frame could be adjusted to account for the angle of the test subject as it entered the catcher. The angle (θ in Figure 18) was set to 60° initially with the intent that it would be changed based on the orientation of the PMHS in the first test.

Steel hooks were attached at one foot intervals along each side of the frame. Pre-ripped strips of fabric were then attached to these steel hooks. Vinyl-coated polyester was the material chosen for the strips due to its relatively high shear strength. The fabric strips were designed to begin tearing as soon as the subject started to load the catcher net. An energy analysis was used to evaluate roughly how many strips were needed to decelerate the subject. A factor of safety was implemented into the design to ensure that the subject would not tear all the strips. Once all of the tear strips were attached to the frame, the other sides of the pre-ripped strips were then attached to a square 10 ft (3 m) heavy-duty nylon personnel safety net (Figure 19). The net and the strips were designed to absorb the majority of the energy of the subject.

The net was implemented to decelerate the subject. However, after deceleration it was assumed that the test subject would fall under gravity to the base of the catching structure. To ensure the subject was protected against further injuries, an additional padding scheme was implemented to cover the plywood base. Small 5 gallon (19 liter) plastic cubic containers and 36 in. x 18 in. (roughly 0.5m x 1m) packaging air bags were utilized as the components of this scheme. A ½" (13mm) hole was drilled into the tops of the plastic cubes to allow air to vent as the cubes deformed under loading. Also, the packaging air bags were only partially inflated so that they could absorb energy before bursting.

The catching mechanism proved effective in decelerating the anthropometrically correct rescue dummy during preliminary tests (Figure 20).
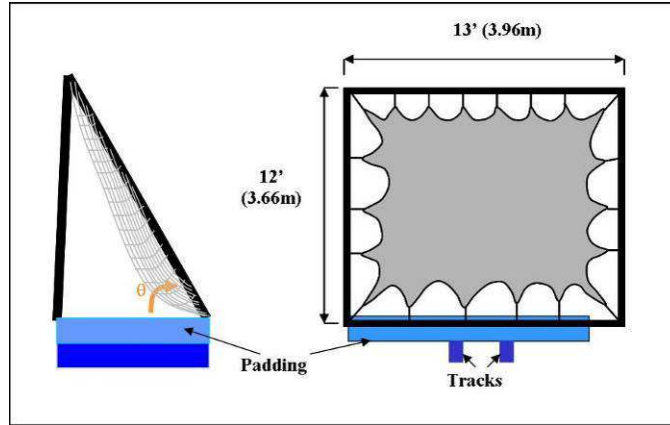
Figure 18: Side (left) and frontal (right) view of catching mechanism.

Figure 19: Energy absorbing strips attached to catcher frame and net.

Figure 20: Preliminary tests showing final position of dummy in the catching mechanism: along track view (left) and side view (right).

FULL SCALE TEST METHODOLOGY FOR PMHS TESTS

After several preliminary tests with rescue dummies were successfully completed, a pilot full scale PMHS test was performed. The following section outlines methodological specifics with respect to this test.

Cadaver Specimen Instrumentation and Preparation

Pretest Cadaveric Specimen Preparation. One unembalmed female human cadaver (163 cm stature, 125 lbs) was obtained and treated in accordance with the ethical guidelines approved by the Human Usage Review Panel, National Highway Traffic Safety Administration, and all PMHS testing and handling procedures were approved by the University of Virginia (UVA) institutional review board. Pre-test CT scans were used to confirm the absence of pre-existing fractures, lesions and other bone pathology in all skeletal structures. All PMHS were preserved by a combination of refrigeration and freezing (Crandall, 1994).

Approximately four days prior to testing, the PMHS was removed from the freezer and allowed to thaw at room temperature over a three day period. Approximately one day before the test, the specimen preparation began. Hardware mounts used to mount instrumentation to skeletal tissues were fitted to the head, first thoracic vertebra (T1), eighth thoracic vertebra (T8) (corresponding to the thorax CG), first lumbar vertebra (L1), center of the sacrum (corresponding to the pelvis CG), bilateral distal femora, bilateral proximal tibiae, and bilateral distal tibiae. A specially designed jig was used to cut out a section of the left femur, and replace that section with hardware designed to hold a femoral load cell in line with the shaft of the femur. The methodology used to install the hardware and, eventually, the load cell is based on a similar methodology used to install load cells in tibiae discussed in Funk et al. 2002.

Test Day Cadaveric Specimen Preparation. On the day of testing instrumentation was mounted to the specimen on the hardware installed during preparation. The specimen was instrumented with a total of eight tri-axial accelerometer arrays, and three 6 degrees-of-freedom (6-DOF) cubes, and a 6-axis femoral load cell (Model 6166, Robert A. Denton Inc., Rochester Hills, MI). Each accelerometer cube and 6-DOF cube contains three accelerometers (Model 7264B-2000, Endevco Corp., San Juan Capistrano, CA) mounted orthogonally. Each 6-DOF cube also contained 3 magnetohydrodynamic (MHD) angular rate sensors (Model ARS-06, ATA Sensors, Albequerque, NM) also mounted orthogonally. The six sensors in each 6-DOF cube were arranged on a common cube mount to allow measurement of both accelerations in, and angular velocities about, each of the three orthogonal axes. The femoral load cell was inserted into the mounting hardware of the left femur (see Funk et al. 2002 for more information regarding in-bone load cells).

Accelerometer cubes were installed on the spine at the T8 and L1 locations. Accelerometer cubes were also installed bilaterally at the junction of the middle and distal third portions of each femur, at the junction of the proximal and middle third portions of each tibia, and at the junction of the middle and distal third portions of each tibia. All lower extremity accelerometer cubes were mounted posteriorly. The three 6-DOF cubes were mounted posteriorly at the head, T1 and sacral hardware locations.

The location of the head CG was found by first marking the Frankfurt planes on the PMHS' head. The lateral projections of the head CG were marked at a location 8.5 mm anterior to the tragion and 25% of the vertical distance from the Frankfurt plane to the top of the head above the Frankfurt plane (Robbins, 1983). The posterior projection of the head CG was marked at a location determined by bisecting a head exterior contour that connected the two lateral projections of the head CG. The 6-DOF cube mounted on the head was mounted at this posterior CG projection.

The three 6-DOF cubes (18 data channels), 8 accelerometer cubes (24 data channels) and the femoral load cell (6 data channels) were connected to a portable wireless data acquisition system (TDAS G5, DTS Inc., Seal Beach, CA) capable of sampling 64 data channels at 10 kHz for 60 seconds. The TDAS system had already been enclosed and padded in a waterproof bag. The padding and enclosure were used to prevent damage to the data acquisition system during the impact and during disinfection.

When the instrumentation installation process was completed, the cadaver was dressed in an inner layer of Tyvek® clothing to help contain the discharge of body fluid, followed by an outer layer consisting of tight-fitting cotton thermal underwear to ensure a realistic interaction between the subject and vehicle.

The specimen's wrists were bound anteriorly with a cable tie, with the left wrist closest to the body and the right wrist farthest from the body (as described in the "Securing The Arms" section above). Lastly, low-top tennis shoes were placed on the subject's feet to more realistically simulate the foot-ground interaction in a pedestrian-vehicle collision.

Surrogate Positioning and Final Test Preparations. The PMHS was then supported via the seat belt straps mentioned in the "Pedestrian Supporting and Release" section above. A cable-pulley system was

connected to the seat belt strap harness and the specimen was hoisted over the pedestrian sled. The PMHS was positioned accordingly following the procedures outlined in the "Pedestrian Stance and Positioning" section.

The PMHS was now in the final position before being struck by the vehicle buck. At this time, a 3-D digitizer, or FARO arm, (Model B08-02, FARO Technologies Incorporated, Lake Mary, FL) was used to record various points on the specimen as well as the locations and orientations of the instrumentation cubes. These points were used to document the overall stance of the subject prior to impact. The locations of the digitized points were used to determine measurements corresponding to the initial position of the PMHS (Figure 21, and Table 1).
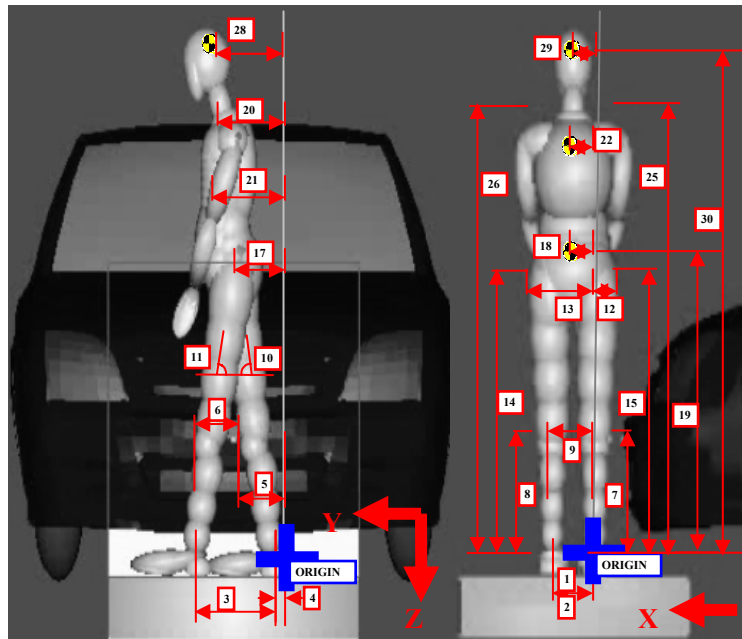

Figure 21. Measurements schematic for pre-test PMHS position (Table 1) prior to the vehicle impact.

Table 1. Measurements describing pre-test position of the PMHS. The *x* direction is defined as the horizontal direction perpendicular to the vehicle motion. The *y* direction is defined as the direction of vehicle motion, and *z* is up and down.

Dimension #	Name	Measurement (mm)	Dir.
1	Heel to Heel Width	198.8	x
2	2nd Metatarsal Width	260.4	x
3	Malleolus Width	225.7	y
4	Right Malleolus Lead	61.3	y
5	Right Patella Lead	-48.8	y
6	Patella to Patella Distance	68.6	y
7	Right Tibial Plateau Height	-402.2	z
8	Left Tibial Plateau Height	-386.4	z
9	Center Patella Distance	242.4	x
10	Right Thigh Angle	80.0 (degrees)	y-z
11	Left Thigh Angle	73.4 (degrees)	y-z
12	Right Greater Trochanter to Ref.	211.6	x
13	Left Greater Trochanter to Ref.	577.2	x
14	Left Greater Trochanter Height	-805.6	z
15	Right Greater Trochanter Height	-806.3	z
16	Right AP Gr. Troch. Dist. To Ref.	-119.4	y
17	Left AP Gr. Troch. Dist To Ref.	-97.9	y
18	Pelvis CG To Ref. (ML)	395.7	x
19	Pelvis CG Height	-875.1	z
20	Right Prox. Ulna To Ref	-2.75	y
21	Left Prox. Ulna To Ref	-18.9	y
22	Thorax CG to Ref	388.5	x
23	Right Prox. Ant Hum. To Ref	-73.9	y
24	Left Prox. Ant Hum. To Ref	-82.2	y
25	Left Shoulder Height	-1373.0	z
26	Right Shoulder Height	-1362.6	z
27	Right Head CG to Ref (AP)	-76.9	y
28	Left Head CG to Ref (AP)	-93.6	y
29	Head CG to Ref (LM)	401.8	x
30	Head CG Height	-1526.4	z

Meanwhile, the catching mechanism was appropriately configured for the mass of the PMHS. The data acquisition system for all the instrumentation was readied and waiting for trigger. Once everything had been determined to be properly functioning, the sled was filled to the corresponding pressure that would yield the desired impact speed of 40 km/h. The PMHS subject was released from the support hardware approximately 30 ms before it was then impacted by the vehicle and thrown into the catcher system. After the test, an autopsy was conducted to assess the extent of the injuries endured by the PMHS.

RESULTS

Coordinate System

The coordinate system used for all measurements and data in this section is defined as the SAE coordinate system with respect to the standing pedestrian. This includes all of the trajectory data (from video analysis), and 6 degrees-of-freedom cube data. This coordinate system is defined as Z positive in the down

direction, X positive anterior to the pedestrian, and Y positive to the right of the pedestrian. Note that the vehicle travels in the –Y direction.

Video Analysis

Analysis of pedestrian surrogate kinematics during the impact event was performed using high speed video images taken from an off-board camera on the vehicle left hand side during all of the tests. The camera used to capture the high speed video (Phantom V5.0, Vision Research, Wayne, NJ) sampled 1024 pixel by 1024 pixel (1.0 mega pixel) images at 1000 Hz during all of the tests.

The locations of each of 5 photo targets on the vehicle, head, T1, T8, and L1 were digitized in every fourth (4th) image, in pixels, from the high speed video data. The spatial resolution of the imager (3.66 mm/pixel) was multiplied by the pixel locations to produce the raw trajectory data. A different pixel resolution was used to determine the raw trajectories for the pedestrian body segments than for the vehicle motion (3.37 mm/pixel) due to the difference in distance between the camera and the outer vehicle plane and between the camera and the vehicle center plane.

Once the raw trajectory data was obtained each signal was shifted in space so that each trajectory began at a (0,0) location in the y-z plane. At this time, all of the signals were filtered as per the specification for trajectory data filtering in an ISO document specifying standards for motorcycle crash analysis (ISO TC 22/SC 22/WG 22, 2004). The trajectory data were smoothed with four passes of the specified filter:

$$y_i = \frac{y_{i-1} + 2y_i + y_{i+1}}{4}$$

$$z_i = \frac{z_{i-1} + 2z_i + z_{i+1}}{4}$$

Eqs.(1)

where y_i and z_i are the y and z coordinates of each target at a time $t=i$. Once the data were filtered, each of the pedestrian's body segment trajectories was subtracted from the vehicle trajectory to produce each body segment trajectory with respect to the vehicle motion. Finally, each signal was shifted in space to a new coordinate system. This coordinate system has an origin at the location defined by the pedestrian ground level in the z direction and by the pedestrian's head photo target in the y-direction. Thus, for instance, in the finalized trajectory data (Figure 22), the head trajectory begins at $(0,h_{zpt})$ where h_{zpt} is the height of the head photo target at time zero.
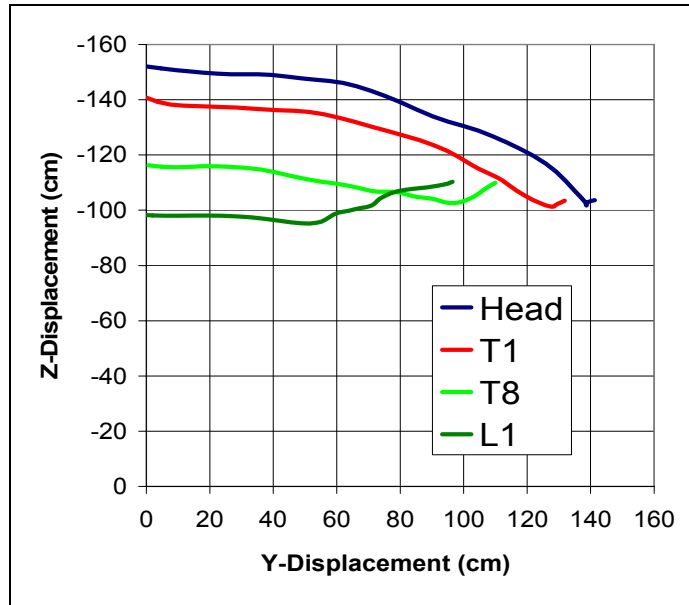

Figure 22: Final trajectories of PMHS test subject.

6-DOF Cube Analysis

Additional kinematics analysis was performed by converting data measured at the 6-DOF cubes to the global coordinate frame.

The routine to find the motion of the cubes in the global reference frame started with determination of the initial position and orientation of the local cube coordinate system (1,2,3) in the global frame (X,Y,Z). Once the test subject was positioned for the impact, coordinates on each cube were digitized with a FARO arm. From these coordinates, the position and orientation of each cube was known, and the initial transformation matrix, $\mathbf{T_0}$, from the global (SAE) frame to the local (cube) coordinate system was determined.

The inverse of $\mathbf{T}$, also the transpose of $\mathbf{T}$ due of orthogonality, represents the transformation from the local (cube) coordinate system to the global (SAE) frame. The transformation matrix, $\mathbf{T}$, will be recalculated at each time step, i, to give $\mathbf{T_i}$, which will describe the orientation of the cube in the global frame throughout the duration of the test. Knowledge of the transformation matrix at each time step allows global rotations and translations, as well as their respective time derivatives, to be calculated for the entire event.

It has been shown that $\mathbf{T_0}$ is determined from the initial position measurements. The procedure to calculate the subsequent $\mathbf{T_i}$ matrices requires input from the angular rate sensors, and involves transforming the previous $\mathbf{T}$ matrix by the incremental rotation matrix at each time step. At any time step, t_i, the angular rates about the three cube axes are known as $\omega_{i,1}$, $\omega_{i,2}$, and $\omega_{i,3}$. The incremental rotation matrix is found by first averaging the angular rates from time t_i and t_{i-1}, which give $\omega_{av,1}$, $\omega_{av,2}$, and $\omega_{av,3}$ as well as an overall magnitude, $\omega_{av,mag}$, for the rotation:

$$\varpi_{av,mag} = \sqrt{\varpi_{av,1}^2 + \varpi_{av,2}^2 + \varpi_{av,3}^2}$$

Eq. (2)

These averaged values are then used to determine the direction vectors, n_i, and angle, ϕ, for the incremental rotation:

$$n_j = \frac{\varpi_{av,j}}{\varpi_{av,mag}}, \qquad j = 1,2,3$$

Eq. (3)

$$\phi = (t_i - t_{i-1})\varpi_{av,mag}$$

Eq. (4)

Euler parameters can be used to describe a rotation about an arbitrary axis. The parameters, e_0, e_1, e_2, and e_3, for the instantaneous rotation are:

$$e_0 = \cos(\frac{\phi}{2})$$

Eq. (5)

$$e_j = n_j \sin\left(\frac{\phi}{2}\right), \qquad j = 1,2,3$$

Eq. (6)

The Euler parameters are then used to determine the rotation matrix, $\mathbf{A}$, for the given instantaneous rotation. The individual components of $\mathbf{A}$, a_{ij}, are calculated using (where the Einstein summation convention is used in the $e_k e_k$ term):

$$a_{ij} = \delta_{ij}(e_0^2 - e_k e_k) + 2e_i e_j + 2\varepsilon_{ijk} e_0 e_k$$

Eq. (7)

At time t_i, the transformation matrix, $\mathbf{T_i}$, is calculated by multiplying the instantaneous rotation matrix, $\mathbf{A}$, by the transformation matrix from the previous time step, $\mathbf{T_{i-1}}$.

$$\mathbf{T_i} = \mathbf{A T_{i-1}}$$

Eq. (8)

Now that the transformation matrices for each time step have been found, the angular rate sensor data can be transformed to the global frame to determine the cube motion in the global coordinate system. The angular rates in the global frame, $\omega_{i,x}$, $\omega_{i,y}$, and $\omega_{i,z}$, are found by multiplying T_i^{-1} by the angular rates in the cube frame, $\omega_{i,1}$, $\omega_{i,2}$, and $\omega_{i,3}$.

$$\begin{bmatrix} \varpi_{i,x} \\ \varpi_{i,y} \\ \varpi_{i,z} \end{bmatrix} = \mathbf{T_i}^{-1} \begin{bmatrix} \varpi_{i,1} \\ \varpi_{i,2} \\ \varpi_{i,3} \end{bmatrix}$$

Eq. (9)

The same transform can be applied to the linear accelerations made in the cube reference in order to determine the accelerations of the cube in the global frame. If $a_{i,1}$, $a_{i,2}$, and $a_{i,3}$ are the local accelerations measured in the cube frame, the accelerations in the global frame, $a_{i,x}$, $a_{i,y}$, and $a_{i,z}$, are found by:

$$\begin{bmatrix} a_{i,x} \\ a_{i,y} \\ a_{i,z} \end{bmatrix} = \mathbf{T_i}^{-1} \begin{bmatrix} a_{i,1} \\ a_{i,2} \\ a_{i,3} \end{bmatrix}$$

Eq. (10)

After the angular rate and acceleration data have been transformed to the global frame, the signals can be integrated to determine rotations, linear velocities, and linear displacements. The global frame rotation and rotational velocity of the cube mounted at the posterior projection of the head CG are given in Figure 23.

Accelerometer Cubes. The resultant acceleration was calculated for each of the 8 accelerometer cubes. Resultant acceleration signals show that peaks in the pelvic and thoracic CG accelerations are comparable whereas the peak in the head acceleration is more than three times greater than those for the thorax and pelvic CGs (Figure 24). Acceleration measurements from the lower extremities (Figure 25) show that both the right and left lower extremities experienced a peak in the acceleration of the distal femur first, followed by a peak in acceleration of the proximal tibia (about 5 ms later) and finally an acceleration in the distal tibia. Peaks in the accelerations of the right lower extremity were greater than accelerations of the left lower extremity, although the distal femur accelerations were comparable.
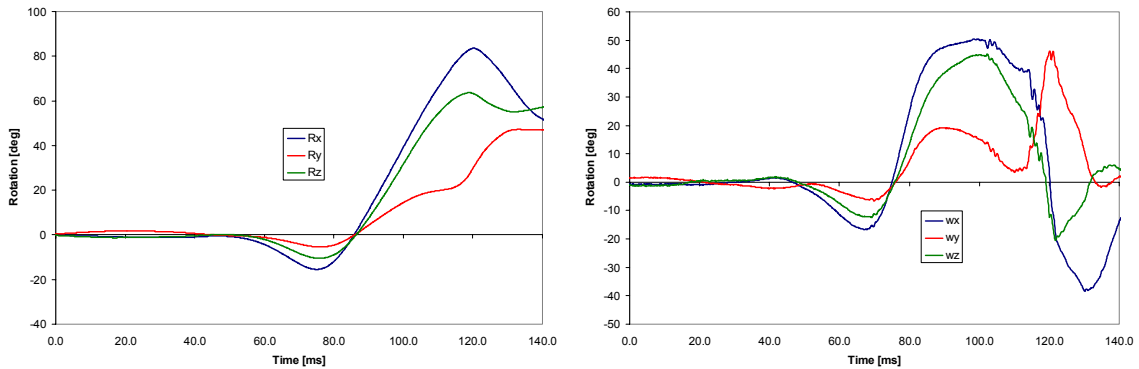

Figure 23: Rotation (left) and angular velocity (right) of the head as measured by the 6-DOF cube in the global coordinate frame.
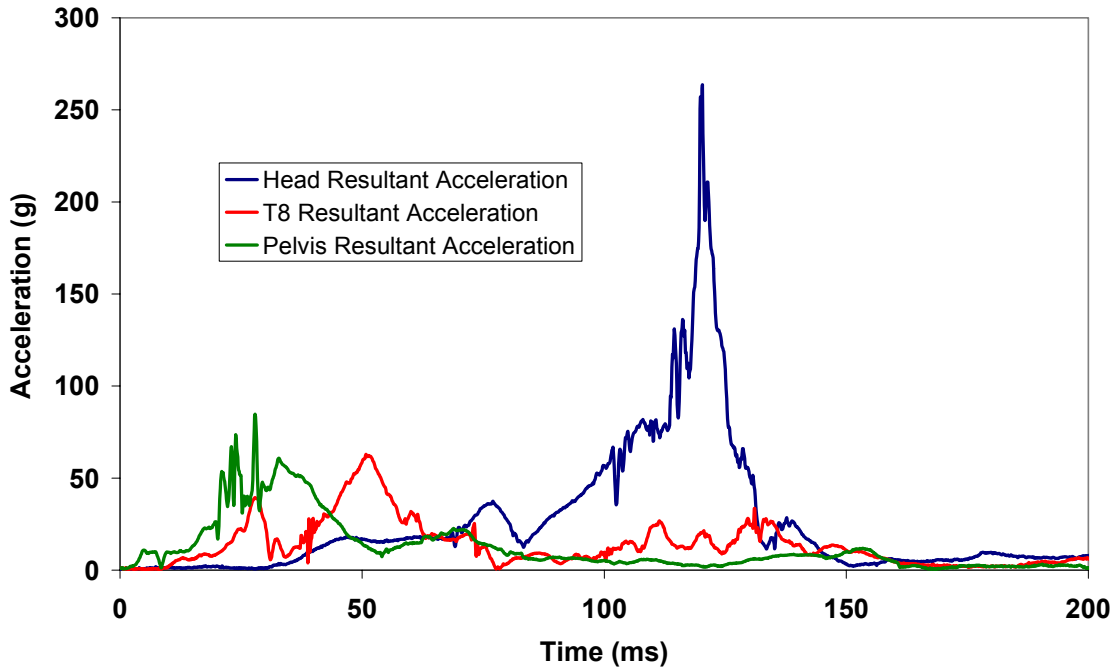
Figure 24: Resultant accelerations from the head, T8 and pelvic accelerometer cubes.
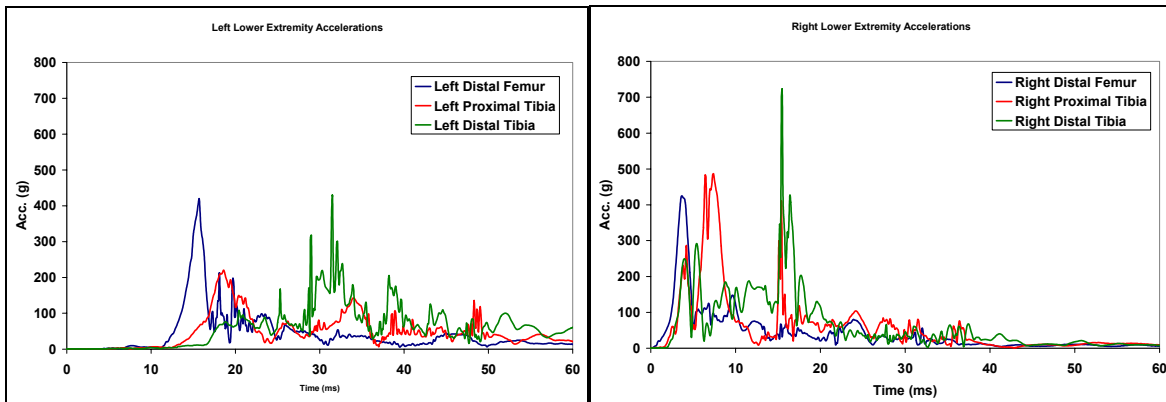

Figure 25: Lower extremity accelerations from the left (on left) and right (on right) lower extremities.

CONCLUSIONS

The goal of this study was to develop an experimental design and test system that would permit controlled full-scale tests on PMHS and pedestrian dummies. This study utilized existing test procedures, real world data and computational simulations to create an experimental test system that is both easy to setup and permits consistently reproducible testing. The system was used successfully in a series of rescue dummy tests, and finally in a pilot full-scale pedestrian impact test with a PMHS.

For our system, the pedestrian is impacted right laterally by an experimental mid-sized sedan traveling at 40km/h (25mph). The pedestrian is positioned in a mid-gait stance (35 to 60 cm stride) with the struck limb back and the hands are bound in front. A simple seat belt system is used to support the upper body and head. This support system is attached to an electromagnetic release mechanism which is triggered to release by the vehicle right before impact.

A pedestrian sled was constructed for the purpose of keeping the correct ground reference level and also for the pedestrian to stand on. The pedestrian sled was equipped with brakes so that the sled would remain stationary as the pedestrian was impacted, but also allowing for the sled to move once the vehicle buck contacts the sled.

A hydraulic piston is used to decelerate the vehicle at the end of the tracks. At this time, the pedestrian continues to move forward (thrown off vehicle) and into our catching mechanism. This catcher was designed to exclude secondary injuries due to impact with the ground by absorbing most of the pedestrian's kinetic energy. The catching mechanism proved effective in stopping the subject after it was thrown off the vehicle.

This paper shows that with the aid of previous full-scale tests, PCDS data, and MADYMO simulations, a successful test setup was designed for full-scale testing of pedestrians.

REFERENCES

ALLARD, P., LACHANCE, R., AISSAOUI, R., SADEGHI, H., and DUHAIME, M. (1997). Able-bodied Gait in Men and Women. *Three-dimensional Analysis of Human Locomotion*. Edited by P. Allard, A. Cappozzo, A. Lundberg and C. Vaughan.

ASHTON, S. J., CESARI, D., and VAN WIJK, J. (1983). "Experimental reconstruction and mathematical modeling of real world pedestrian accidents". Birmingham University, Accident Research Unit (England)/ Organisme National de Securite Routiere, Laboratoire des Chocs et de Biomecanique, Bron, France/ Institut TNO voor Wegtransportmiddelen, Delft, Netherlands/ National Highway Traffic Safety Administration, Vehicle Research and Test Center, East Liberty, Ohio. 19 p. Pedestrian Impact - Injury and Assessment. Warrendale, Pa., SAE, February 1983, p. 205-223. Sponsor: Transport and Road Research Laboratory, Crowthorne, England. Report No. SAE 830189. UMTRI-48288 A18.

BILLAULT, P., BERTHOMMIER, M., GAMBARELLI, J., GUERINEL, G., FARISSE, J., SERIAT-GAUTIER, G., DAOU, N., BOURRET, P., CAVALLERO, C., CESARI, D., and RAMET, M. (1981). "Pedestrian safety improvement research". Citroen SA, Velizy, France/ Marseille Laboratoire d'Anatomie, France/ Organisme National de Securite Routiere, Laboratoire des Chocs et de Biomecanique, Bron, France. 15 p. International Technical Conference on Experimental Safety Vehicles. Eighth [Proceedings]. Washington, D.C., NHTSA, 1980, p. 822-836. UMTRI-46767 A58.

BOURRET, P., FARISSE, J., SERIAT-GAUTIER, B., LAROUSSE, R., BILLAULT, P., RAMET, M., CESARI, D., and CAVALLERO, C. (1979). "Experimental study of injuries observed on pedestrians". Hopital de Salon-de-Provence, France/ Marseille Laboratory of Anatomy, France/ Citroen SA, Paris, France/ Organisme National de Securite Routiere, Laboratoire des Chocs, Bron, France. 12 p. Cotte, J. P., and Charpenne, A., eds. International IRCOBI Conference on the Biomechanics of Trauma, 4th Proceedings. Bron, IRCOBI, 1979, p. 263-274. UMTRI-42962 A22.

BRUN-CASSAN, F., VINCENT, J. C., TARRIERE, C., FAYON, A., CESARI, D., CAVALLERO, C., and MAURON, G. (1984). "Comparison of experimental car-pedestrian collisions performed with various modified side-impact dummies and cadavers". Peugeot-Renault Association, Laboratoire de Physiologie et de Biomecanique, Rueil-Malmaison, France/ Organisme National de Securite Routiere, Bron, France/ Peugeot Automobiles, Centre d'Etudes, Paris, France. 11 p. Stapp Car Crash Conference. Twenty-Eighth Proceedings. Warrendale, Society of Automotive Engineers, November 1984, p. 149-159. Report No. SAE 841664. UMTRI-71157 A10.

CAVALLERO C., CESARI D., RAMET M., BILLAULT P., FARISSE J., SERIAT-GAUTIER B., and BONNOIT J. (1983). "Improvement of pedestrian safety: influence of shape of passenger car-front structures upon pedestrian kinematics and injuries: evaluation based on 50 cadaver tests". Organisme National de Securite Routiere, Laboratoire des Chocs et de Biomecanique, Bron, France/ Citroen SA, Velizy, France/ Marseille Laboratoire d'Anatomie, France. 13 p. Pedestrian Impact - Injury and Assessment. Warrendale, Pa., SAE, Feb. 1983, p. 225-237. Report No. SAE 830624. UMTRI-48288 A19.

CESARI, D., RAMET, M., CAVALLERO, C., BILLAULT, P., GAMBARELLI, J., GUERINEL, G., FARISSE, J., SERIAT-GAUTIER, B., and BOURRET, P. (1980). "Experimental study of pedestrian

kinematics and injuries". International IRCOBI Conference on the Biomechanics of Impacts, 5th Proceedings.

CHIDESTER, A. and ISENBERG, R. (2001). Final Report – The Pedestrian Crash Data Study. National Highway Traffic Safety Administration. United States of America. Paper Number 248.

COMMUNITY ROAD ACCIDENT DATABASE (CARE). EUROPA, European Commision, Transport. http://europa.eu.int/comm/transport/care/statistics/most_recent/detailed_breakdown/index_en.htm. (2002). (Accessed April 15, 2004).

CRANDALL J. (1994). The Preservation of Human Surrogates for Biomechanical Studies. PhD Dissertation released by the University of Virginia Department of Mech. and Aero. Engineering.

EUROPEAN ENHANCED VEHICLE-SAFETY COMMITTEE, "EEVC Working Group 17 Report— Improved Test Methods to Evaluate Pedestrian Protection Afforded by Passenger Cars". www.eevc.org, December 1998.

FARISSE, J., SERIAT-GAUTIER, B., DALMAS, J., DAOU, N. FACULTE DE MEDECINE DE MARSEILLE. BOURRET, P., CAVALLERO, C., CESARI, D., RAMET, M. ONSER, BRON. and BILLAULT, P., Berthommier, Citroen, Velizy. (1981). "Anatomical and Biomechanical Study of Injuries Observed During Experimental Pedestrian-Car Collisions". 6th IRCOBI – Salon-de-Provence.

FUNK, J., RUDD, R., SRINIVASAN, S., KING, R., CRANDALL, J., and PETIT, P. (2002). "Methodology for measuring tibial and fibular loads in a cadaver". SAE 2002 World Congress, SAE Paper #2002-01-0682.

HEGER, A. and APPEL, H. (1981). "Reconstruction of pedestrian accidents with dummies and cadavers". Berlin Technische Universitaet, Institut fuer Kraftfahrzeuge, Germany FR. 6 p. International Technical Conference on Experimental Safety Vehicles. Eighth [Proceedings]. Washington, D.C., NHTSA, p. 836-841. UMTRI-46767 A59.

HENARY, B., CRANDALL, J., BHALLA, K., MOCK, C., and ROUDSARI, B. (2003). "Child and Adult Pedestrian Impact: The Influence of Vehicle Type on Injury Severity". 47th Annual Proceedings, Association for the Advancement of Automotive Medicine, September 22-24, 2003.

ISHIKAWA, H., KAJZER, J., and SCHROEDER, G. (1993). "Computer simulation of impact response of the human body in car-pedestrian accidents". Japan Automobile Research Institute, Ibaraki/ Chalmers Tekniska Hoegskola, Goeteborg (Sweden)/ Hannover Medical University, Germany. 14 p. Stapp Car Crash Conference. Thirty-seventh Proceedings. Warrendale, SAE, November 1993, p. 235-248. Report No. SAE 933129. UMTRI-84831 A18.

ISO TC 22/SC 22/WG 22. (2004). Motorcycles—Test and analysis procedures for research evaluation of rider crash protective devices fitted to motorcycles—Part 4: Variables to be measured, instrumentation, and measurement procedures, AND Part 5: Injury indices and risk/benefit analysis. ISO Document Numbers ISO/DIS 13232-4, and ISO/DIS 13232-5.

KALLIERIS, D. and SCHMIDT, G. (1988). "New aspects of pedestrian protection loading and injury pattern in simulated pedestrian accidents". Heidelberg Universitaet, Germany FR. 12 p. Stapp Car Crash Conference. Thirty-Second Proceedings. Warrendale, SAE, October 1988, p. 185-196. Report No. SAE 881725. UMTRI-77800 A13.

KELLEHER, B.J., WALSH, M.J., VERGARA, R.D., HERRIDGE, J.T., and EPPINGER, R.H. (1986). "Evaluation of a pedestrian-compatible bumper". Calspan Corporation, Buffalo, N.Y./ Battelle, Columbus, Ohio/ National Highway Traffic Safety Administration, Washington, D.C. 12 p. International Technical Conference on Experimental Safety Vehicles. Tenth [Proceedings]. Washington, D.C., NHTSA, February 1986, p. 1023-1034. UMTRI-77089 A72.

MEISSNER, M., VAN ROOIJ, L., BHALLA, K., CRANDALL, J., LONGHITANO, D., TAKAHASHI, Y., DOKKO, Y., and KIKUCHI, Y. (2004). "A Multi-Body Computational Study of the Kinematic and Injury Response of a Pedestrian with Variable Stance upon Impact with a Vehicle". SAE 2004 World Congress, SAE Paper #2004-01-1607.

NATIONAL HIGHWAY TRAFFIC SAFETY ADMINISTRATION (NHTSA). (2003). "Traffic Safety Facts 2003-Pedestrians". DOT HS 809 769.

NATIONAL POLICE AGENCY (Japan). Traffic Accidents Situation 2003. Fatalities by Age Group and Road User Type. http://www.npa.go.jp/english/index.htm. (2003). (Accessed April 12, 2004).

PERRY, J. (1992). *Gait Analysis: Normal and Pathological Function.* SLACK Incorporated, NJ.

PRITZ, H.B., HASSLER, C.R., HERRIDGE, J.T., and WEIS, E.B., Jr. (1975). "Experimental study of pedestrian injury minimization through vehicle design". Battelle Memorial Institute, Columbus Laboratories, Ohio. 27 p. Stapp Car Crash Conference. Nineteenth. Proceedings. Warrendale, Society of Automotive Engineers, p. 725-751. Report No. SAE 751166. UMTRI-33279 A26.

ROBBINS, D.H. (1983). Anthropometric Specifications for Mid-Sized Male Dummy, Volume 2. University of Michigan Transportation Research Institute (UMTRI), report number UMTRI-83-53-2. Dec. 1983.

SCHROEDER, G., KONOSU, A., ISHIKAWA, H., and KAJZER, J. (2000). "Injury Mechanism of Pedestrians During a Front-End Collision with a Late Model Car". JSAE Spring 2000.

WINTER, D.A. (1990). *Biomechanics and Motor Control of Human Movement.* John Wiley & Sons Inc.

The World Bank Group. Road safety. www.worldbank.org/html/fpd/transport/roads/safety.htm. (2002). (Accessed March 8, 2004).

DISCUSSION

PAPER: **Full Scale Pedestrian Impact Testing with PMHS: A Pilot Study**

PRESENTER: *Jason Kerrigan, University of Virginia Center for Applied Biomechanics and*
                          General Motors

QUESTION: *Erik Takhounts, NHTSA*
        How representative is that case to what happens actually in the real world to pedestrians?

ANSWER: Representative in terms of injuries?

Q: In terms of size of the pedestrians and in terms of injuries, yes.

A: In terms of size of the pedestrians.

Q: Yeah, yeah. As you know, it seems to be the geometry—two contacting geometries will drive where
        the injuries will occur.

A: Um hm. So I actually did do a little slide here, but—

Q: Oh. You already knew my question.

A: I was already prepared actually. If we look at AIS-2, 2+ injuries in pedestrians: 31% are head injuries
        and 32% are lower extremity injuries. If you look at the top 10 injuries caused by, 10 injuries, which is
        from the PCDS, we noticed that in this particular case, we did see six of those injuries.

Q: Okay. Now, your cadavers seem to have all of them. And unless you are going to make cars out of
        rubber, how are you going to—What are you going to try to propose?

A: I'm not—I'm definitely not trying to propose a solution for car manufacturers that prevent injuries to
        pedestrians. We're just trying—

Q: Well, why are you doing your research then?

A: We're trying to figure out what's going on.

Q: But once you figure it out, what's going on, basically everything is injured. You know, that's a no-
        brainer. [laughter] So, what's next? What are we going to do about it?

A: Well, there's—There's a lot of studies that we're working on. We're also looking at things related to
        vehicle geometry and vehicle stiffness. First, the main goal is actually to understand what's going on.
        What parts of the vehicle are too stiff? What parts of the vehicle are not too stiff and how do those
        stiffnesses affect head injuries and those sorts of issues. In this case, yes, this car was actually, caused
        significant injuries to pedestrians, but I'd say this is not a representative vehicle of the fleet also because
        a lot of the vehicles that are going to be sold in Europe in 2005 will have to pass some EEVC
        regulations regarding pedestrian safety. So, we're just taking it—This is a pilot study presenting the
        fact that we're actually able to do this research. We're learning things here as we go along. And,
        you're right. I cannot say, you know, I'm not a vehicle manufacturer. I'm not a design engineer, so I
        don't know what we will actually suggest for the vehicle. So.

Q: Okay. Thanks.

QUESTION: *Steve Rouhana, Ford Motor Company*
        I'm curious: The initial set-up of the cadavers, especially given the fact that you were interested in
        kinematics. You had their hands bound. That's going to change your rotational inertia of the body with
        respect to, around the X-axis.

ANSWER: Yes.

Q: May not be that much because you're only dealing with the forearms and hands, but it's also going to place interesting initial conditions and boundary conditions on the whole body as it's rotating. Can you comment on that?

A: Sure. We've actually done quite a bit of modeling before we actually ran these tests looking at what's going on in the upper extremities. As I had shown for one of the top 10 most frequent injuries is the humorous fracture. Now, we don't really understand what's going on, but what we've seen for most of the modeling is there's really two situations that can occur: This upper extremity can get pinned between the thorax and the car and actually take a brunt of the load in the elbow, the humorous, the shoulder and actually—That actually slows down or makes the head impact a lot less. So, that's one case that can happen. The other case that happens is that elbow actually goes a little anterior to the body and it stretches the arm across the chest like that, and then the arms are basically taken out of the picture here. So, we've got two things going on. We really got to kind of choose what we want. And now from some of the things that we looked at from simulations, it seems that that initial position of the arms, it's really, really hard to tell what's actually going to happen in that case. So depending on where you have the arms, you know, even a few millimeters could change how that elbow is loaded, how that upper extremity is loaded. Now so, we talked about this in our SAE paper a little bit, but actually we are interested in this particular case of removing the effect, that effect of the arm to see that whole thorax loading and see that most severe head loading. So in order to do that, we actually bound the arms in front and have found that kind of reduces the potential for variability.

Q: In your modeling, did that—Did that effect, for example, the trajectory of the head?

A: Yeah! Yes, it does because it's—Well, you mean with the arms bound or with—

Q: Yeah. With the arms bound. Well, the difference.

A: Right. So the difference between the two: If the arms are not bound, in some cases the elbow ends up under the thorax and in some cases it doesn't. Well if it actually ends up under the thorax, of course that affects the trajectory because it slows down the whole upper body and the head actually won't actually contact the vehicle because it'll come down and hit the shoulder. So, to answer your question: yes.

Q: Thanks. Nice presentation.

QUESTION: *Guy Nusholtz, DaimlerChrysler*
First a quick question: Is that instrumentation package a similar one to what's being used in the World SID? It looked like from the slide.

ANSWER: That's actually a specially-designed thing. It's three—

Q: No, no, no. I'm sorry. It's the data acquisition.

A: Oh, yes. I believe it's the same one that's in World SID. It's the DTS T-G5 system. We actually have two of those in there giving us 64 channels.

Q: That's the first question. Second is: Did you go through the accident data and find out what is the most common, the most likely accident for pedestrians? Because 40 kilometers per hour seems kind of high.

A: Well, we chose 40 kilometers per hour because that is what the, most of the regulations around the world are being developed at right now. I believe that—I don't have the data actually here, but I believe if you look at a distribution of AIS 3 or 4+ injuries to pedestrians, the peak is somewhere around 40 kilometers per hour also, and really 40 kilometers per hour has kind of been what's come up for all the pedestrian testing that, for all the regulations that will be developed—or, that have been developed in Europe and that are being developed in Japan right now. So, that's the reason why we chose 40.

Q: You may want to consider several speeds. One of the questions is: Do you get different dynamics depending on the speed? If I run it at 20, then when you go and you try and develop a counter measure for that problem, what you do at 20 may be detrimental for 40, or make it worse.

A: Make it much worse at a higher speed. I agree. … The speed of the vehicle could actually contribute to some sliding. I don't know if you saw in the pictures before, but the pelvis actually does quite a bit of sliding as it moves across the [hood]. Totally may be affected by the speed of the vehicle, which completely changes the kinematics, in general. The tests are really that variable, but we have to kind of start with one set and start there, and we can, we move up from there. And, I agree that we do need to look at different speeds because although auto manufacturers are making their cars safe for 40, then, you know, people could be dying at 20.

Q: It could be a—It could be a typical problem. It's one that we face all the time. Just a quick—

A: Guy, you're cuttin' into your time, actually, since you're next.

Q: Oh, okay. Then I'll stop!

QUESTION: *Kelly Kennett, InSciTech Inc.*
This is more just a comment even to what Steve was raising. I don't think you should get caught off splitting hairs about the inertia of the upper extremities. One of the things that happens with these pedestrians is the velocity of pedestrian itself is non-negligible in the way that these kinematics developed. I mean, Guy is right. You know, 25 miles an hour is on the high side. If you look at even a walking velocity—5 miles an hour and an impact of 20 or a dart out of 10, 15, 20—I mean often the pedestrian's velocity itself is half or more of the car's velocity. So to have a standing pedestrian which, you know, which you've tried to imitate weight distribution but yet, I mean the velocity of the pedestrian itself is large relevant to the car. [Right.] And, I think, you know, to get caught up in arms here or arms there or whatever else when, you know, you've kind of—You know, you don't want to measure with a, you know, a micrometer and cut with a butter knife. I mean, exactly.